Adaptive Control of a Nanopositioning Device

Arnfinn Aas Eielsen and Jan Tommy Gravdahl

Abstract— **High-bandwidth tracking control is desirable in many nanopositioning applications, including scanning probe microscopy. Typical nanopositioner designs have several sources of uncertainty which can degrade control performance, and even induce instability. Salient uncertainties are in the control gain and the resonant frequencies of the mechanical structure. The control gain varies due to hysteresis and creep which result in a control gain that is dependent on the offset, range, and form of the driving signal, as well as actuator temperature and age. The resonant frequencies change due to payload mass. In order to maintain performance in the presence of moderately changing dynamic response, a model reference adaptive control (MRAC) scheme is proposed and implemented. The details of implementing a working MRAC will be discussed. Most notably, a novel augmentation of the parameter identification scheme in the form of a special pre-filter, will be shown to be necessary to obtain parameter convergence, and thus also stability in the case of the MRAC scheme. Experimental results are presented to assess the performance.**

I. INTRODUCTION

Nanopositioning is typically associated with scanning probe microscopy (SPM), and its many applications. Some application task typically require general reference trajectory tracking, i.e., for manipulation, fabrication, and lithography. In order to improve throughput in such settings, high bandwidth control is required [1]–[3]. As the dynamic response of typical positioning systems employed has a fair amount of uncertainty, both inherently and due to the specific application, the control laws used also need to have sufficient robustness. Although the dynamic response is uncertain, it is dominantly linear and can be well described by linear ordinary differential equations for specific operating points. These systems should therefore be amenable to adaptive control schemes, which in principle can provide higher and more consistent performance than standard robust static control schemes.

The standard indirect model reference adaptive control (MRAC) framework [4] is used in this work in order to develop a complete adaptive control scheme for a nanopositioning device of common design. As will be demonstrated, there are some important considerations to be made with regards to how to choose the plant model, how to tune the control law, and how to obtain parameter convergence for the adaptive law. The resulting control scheme is believed to be a well performing MRAC. The experimental results should therefore be indicative of the performance that can be expected applying MRAC to this particular type of system.

The main novelty presented is a special pre-filter needed in order to obtain parameter convergence.

This work was supported by the Norwegian Research Council and the Norwegian University of Science and Technology.

Jan Tommy Gravdahl jan.tommy.gravdahl@itk.ntnu.no and Arnfinn Aas Eielsen arnfinn.aas.eielsen@itk.ntnu.no are with the Department of Engineering Cybernetics at the Norwegian University of Science and Technology, Trondheim, Norway.

II. SYSTEM DESCRIPTION AND MODELING

The devices in the system used for the experiments are fairly typical of systems used for motion control in general. The system consists of a positioning mechanism, which is a custom-designed serial-kinematic piezoelectric stack-actuated nanopositioning stage, as well as the necessary instrumentation, including anti-aliasing and reconstruction filters, a piezo voltage amplifier, a capacitive displacement sensor, and a standard hardware-in-the-loop (HIL) system. The HIL system is used to implement the control scheme, and simply described, it is a computer fitted with digital-to-analog (DAC) and analog-to-digital (ADC) converters.

In this section a plant model which includes the dynamics for the nanopositioning stage, as well as the dynamics of the anti-aliasing and reconstruction filters, is presented. A more complete model would also include the amplifier and sensor dynamics, and the time-delay incurred by the zero-order-hold (ZOH) elements in the DAC and ADC. The attainable sampling speed was fast enough for the phase-lag due to the ZOH elements to be insignificant within the bandwidth of the controller, and the amplifier and sensor dynamics is faster than what is possible to represent when using the attainable sampling speed. A very high-order model would also introduce stability and performance issues due to numerics and computational complexity. The plant model presented here is the model which has the highest practically obtainable accuracy for this system. A diagram of the plant model is found in Fig. 1.

A. Mechanical Model

The nanopositioning stage used in this work is shown in Fig. 2. It is a serial-kinematic motion mechanism, designed such that the first vibration mode is dominant and occurs in the actuation direction (piston mode). The simplified free body diagram for the mechanism is displayed in the inset image in Fig. 2, and by this model the corresponding second-order differential equation to describe the dynamics of the displacement w_x (where subscript "x" indicates the x-direction) is given by

$$m_x\ddot{w}_x(t) + c_x\dot{w}_x(t) + k_x w_x(t) = f_x(t)\ ,$$

where m_x (kg) is the mass of the sample platform, as well as any additional mass due an attached payload, c_x (N s m^{-1})

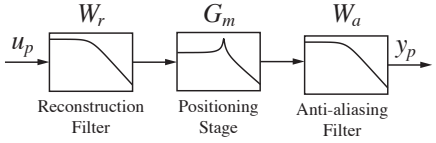

Fig. 1. Plant model.

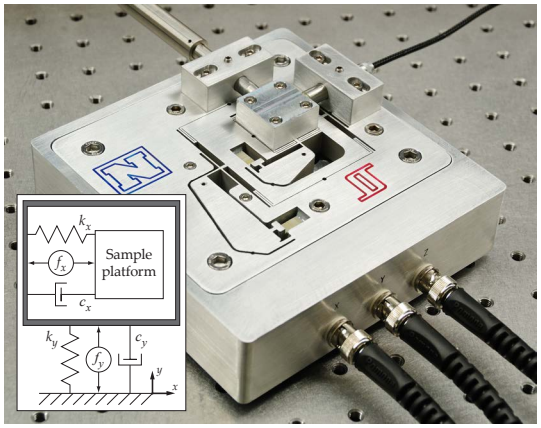

Fig. 2. Serial-kinematic nanopositioning stage.

is the damping coefficient, and k_x (N m^{-1}) is the spring constant. The applied external force from the piezoelectric actuator f_x (N) is

$$f_x(t) = \beta u_a(t) + d_h(t) \,,$$

where β (N V^{-1}) is the effective control gain of the actuator from voltage to force, and u_a (V) is the applied voltage. The actuator will introduce hysteresis and creep when driven by a voltage signal. It is a reasonable assumption to consider this behavior as a bounded disturbance added to the input [5], represented by the term d_h.

Denoting the deflection $y_d = w_x$, the transfer function for the nanopositioning stage is

$$G_m(s) = \frac{y_d}{u_a}(s) = \frac{b_0}{s^2 + a_1 s + a_0} = \frac{b_0}{s^2 + 2\zeta\omega_0 s + \omega_0{}^2} \,, \quad (1)$$

where $b_0 = \beta/m$ (m s^{-2} V^{-1}), $a_0 = k/m$ (s^{-2}), $a_1 = c/m$ (s^{-1}), $\zeta = c/2\sqrt{mk}$ (-), and $\omega_0 = 2\pi f_0 = \sqrt{k/m}$ (s^{-1}).

The frequency response for the x-axis is recorded in two configurations, with and without a payload of approximately 15.7 g attached, using bandwidth-limited white noise excitation. The responses are displayed in Fig. 3. The model (1) is fitted to the frequency response data using the MATLAB System Identification Toolbox, and the resulting parameter values are presented in Table I. The response of the model (1) using these parameters is also displayed in Fig. 3 for comparison.

TABLE I

IDENTIFIED PARAMETERS FOR THE MODEL (1), FOR TWO PAYLOAD CONFIGURATIONS, USING FREQUENCY RESPONSE DATA.

1) With payload on sample platform					
b_0	$1.97{\cdot}10^6$	μm/s^{2}V	b_0/a_0	0.109	μm/V
a_0	$18.1{\cdot}10^6$	1/s^2	f_0	677	Hz
a_1	127	1/s	ζ	0.0149	-
2) Without payload on sample platform					
b_0	$2.33{\cdot}10^6$	μm/s^{2}V	b_0/a_0	0.107	μm/V
a_0	$21.9{\cdot}10^6$	1/s^2	f_0	744	Hz
a_1	131	1/s	ζ	0.0140	-

B. Anti-Aliasing and Reconstruction Filters

The anti-aliasing and reconstruction filters, $W_a(s)$ and $W_r(s)$ respectively, are second-order Butterworth filters, and are chosen to be identical, $W_r(s) = W_a(s)$, for convenience. They have a transfer function of the form

$$W_a(s) = W_r(s) = \frac{\omega_c{}^2}{s^2 + \sqrt{2}\omega_c s + \omega_c{}^2} \,, \quad (2)$$

where ω_c is the cut-off frequency.

As the cut-off frequency ω_c for the anti-aliasing and reconstruction filters used in the experimental setup is user programmable, the filters provide an extra degree of freedom for the control law tuning. The filters can be used to attenuate excitation of non-modeled high-frequency dynamics, as well as quantization and sensor noise. The cut-off frequency selection can also to some degree improve the nominal closed-loop sensitivity response and robustness properties, given that the cut-off frequency ω_c is below the Nyquist frequency.

C. Complete Plant Model

The plant model for the system presented in Fig. 1 is

$$\frac{y_p}{u_p}(s) = H_p(s) = W_a(s) G_m(s) W_r(s) \,.$$

The usage of this model for the design of the MRAC will not provide good performance with respect to the closed-loop sensitivity function, as it will have a finite non-zero DC-gain. Due to external disturbances, such as the ones introduced by the hysteresis and creep non-linearities, and in order to reduce the impact of model uncertainty, it is advisable to add integral action to the controller [6]. The response of the closed-loop sensitivity function at lower frequencies will then improve, and the DC-gain will be zero. This can be done by augmenting the system with an integrator, implemented as part of the control scheme. The plant model used is thus

$$G_p(s) = \frac{1}{s} H_p(s) \,. \quad (3)$$

The overall model order is $n_p = 7$.

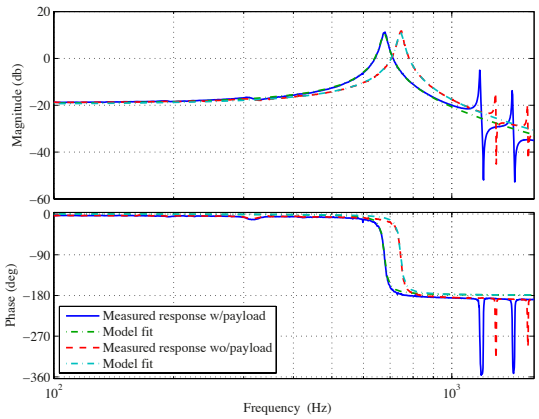

Fig. 3. Measured frequency response and model response, for the two payload configurations, and corresponding model fits.

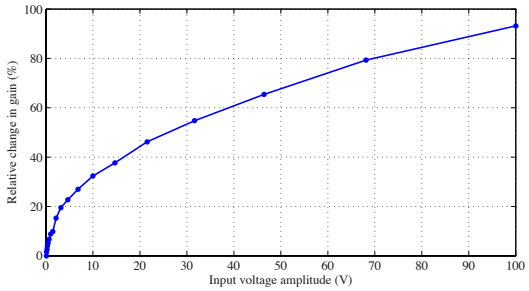

Fig. 4. Relative change in low-frequency gain b_0/a_0 for the piezoelectric actuator due to the input voltage amplitude (when using a 10 Hz sinusoid).

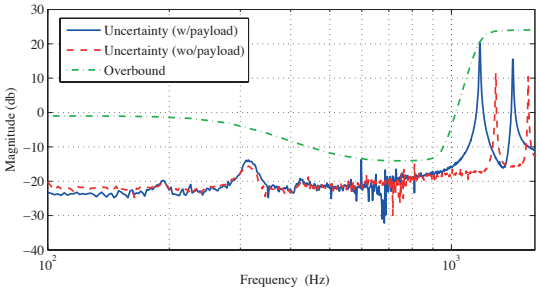

Fig. 5. Open-loop uncertainty weight $\delta_m(s)$, for the two payload configurations and an overbounding approximation.

D. Model Uncertainty

The uncertainty in the nanopositioner dynamics is due to specific user applications, as well as inherent properties in the actuator and mechanical structure.

Users will typically need to position payloads of various masses, and therefore the resonant frequencies and the effective control gain of the mechanical structure will change every time a new payload is attached [7]. This is demonstrated by inspecting the frequency responses for the two payload configurations in Fig. 3, and the corresponding parameter values for the model (1) in Tab. I. As can be seen from Fig. 3, the response of the first vibration mode is well approximated by the second-order model (1) using the identified parameters in Tab. I, for both payload configurations. It is evident that there exist higher order modes in the system, and the second and third vibration modes are clearly visible in Fig. 3. These higher order modes have very small magnitude responses in comparison to the first, and they have shapes and directions that will make them difficult to control using the mounted actuator, thus the only practical solution is to avoid exiting these modes by limiting the bandwidth of the control law.

The majority of nanopositioning designs use piezoelectric actuators, which will have inherent variations in the effective control gain β due to changes in actuator temperature, offset voltage, displacement range, as well as due to depolarization of the piezoelectric actuator [8]–[10]. The hysteresis and creep non-linearities present in all piezoelectric actuators are the main contributors to the change in effective gain, and this is directly dependent on the offset voltage and input voltage amplitude, or displacement range. The dependence on input voltage amplitude is shown in Fig. 4, where the relative change of the low-frequency gain b_0/a_0 is recorded as a function of the amplitude (when using a 10 Hz sinusoid.) The relative change of the gain is found to be over 90% at an amplitude of 100 V compared to the gain at 100 mV.

To assess the nominal robustness of the proposed control scheme, the uncertainty of the mechanical model is taken into account as a multiplicative perturbation to the positioner dynamics,

$$\bar{G}_m(s) = G_m(s)(1+\delta_m(s)\Delta_m(s));\ |\Delta_m(j\omega)| \leq 1\ \forall\ \omega\,. \quad (4)$$

The uncertainty weight $\delta_m(s)$ is determined experimentally for the two payload configurations, and incorporating the uncertainty of the effective gain, an overbounding uncertainty weight is found and shown together the experimentally determined uncertainties in Fig. 5.

III. CONTROL SCHEME DESCRIPTION

As the only measurement available in the system is the displacement of the sample platform, a control scheme for the system must use output-feedback. Readily available adaptive control schemes for output-feedback includes model reference adaptive control (MRAC) [4], $\mathscr{L}_1$ adaptive output-feedback control [11], and adaptive observer backstepping [12]. MRAC and adaptive observer backstepping can provide asymptotic output tracking. $\mathscr{L}_1$ adaptive output-feedback control provides an disturbance observer adapting to the discrepancy between the plant output and a reference model, and the stability and performance will depend on the choice of reference model and a low-pass filter which is non-trivial to find in general. Adaptive observer backstepping is dependent on non-linear damping terms, which can lead to impractically large actuation forces, and also yields unwieldy control laws for higher order system models. The MRAC scheme was deemed to be the most feasible choice. The control law and adaptive law is decoupled, such that they can be designed separately. The design procedures for the control law and adaptive law are also fairly straight forward.

A. Model Reference Adaptive Control

The MRAC scheme consists of a control law and an adaptive law, that can be designed independently and then combined using the certainty equivalence principle [4]. A MRAC scheme can generally be implemented in direct and indirect form. The main difference is that for the direct form, the controller parameters are estimated directly, whereas for the indirect form, the plant parameters are estimated and subsequently mapped to the control parameters. The chosen plant model order is $n_p = 7$, which for the direct case requires $2n_p = 14$ parameters to be estimated. As only three plant parameters, b_0, a_1, and a_0, are uncertain and require estimation, employing an indirect MRAC reduces the complexity and computational requirements of the parameter identification significantly. In addition, experience suggests that parameter convergence is much more difficult to achieve with a larger number of estimated parameters.

B. Control Law

The MRAC objective is to make the plant output y_p perfectly track the output of a reference model y_m. The general model reference control law is summarized below.

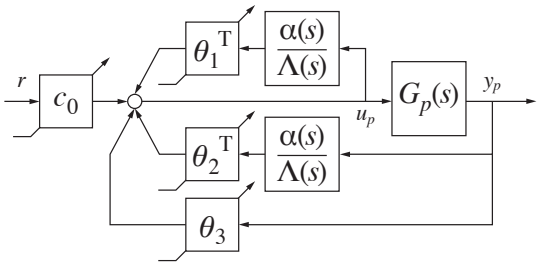

Fig. 6. The MRAC control law structure.

The plant model can be expressed as

$$\frac{y_p}{u_p}(s) = G_p(s) = k_p \frac{Z_p(s)}{R_p(s)} .$$

It is assumed that $R_p(s)$ and $Z_p(s)$ are monic polynomials. The polynomial $Z_p(s)$ is also Hurwitz, and is of degree m_p. In addition, the degree n_p of $R_p(s)$, the relative degree $n^\star = n_p - m_p$ of $G_p(s)$, and the sign of the high-frequency gain k_p are known.

The reference model

$$\frac{y_m}{r}(s) = W_m(s) = k_m \frac{Z_m(s)}{R_m(s)}$$

consists of the monic Hurwitz polynomials $Z_m(s)$ and $R_m(s)$ of degrees q_m and p_m, respectively, where $p_m = n_p$, and the relative degree $n_m{}^\star = p_m - q_m = n^\star$.

The control law, as shown in Fig. 6, is given by

$$u_p = \theta_1{}^{\mathrm{T}} \frac{\alpha(s)}{\Lambda(s)} u_p + \theta_2{}^{\mathrm{T}} \frac{\alpha(s)}{\Lambda(s)} y_p + \theta_3 y_p + c_0 r$$

where

$$\begin{aligned} &\alpha(s) = [s^{n_p-2}, s^{n_p-3}, ..., s, 1]^{\mathrm{T}} && \text{for } n_p \geq 2 \\ &\alpha(s) = 0 && \text{for } n_p = 1 \end{aligned}$$

and

$$\Lambda(s) = \Lambda_0(s) Z_m(s)$$

is a monic and Hurwitz polynomial of degree $n_p - 1$. Thus, $\Lambda_0(s)$ is a monic and Hurwitz polynomial of degree $n_0 = n_p - 1 - q_m$. The control law parameter vector is

$$\theta_c = [\theta_1{}^{\mathrm{T}}, \theta_2{}^{\mathrm{T}}, \theta_3, c_0]^{\mathrm{T}}$$

and should be chosen such that the closed-loop complementary sensitivity function matches the reference model, i.e.,

$$\frac{y_p}{r}(s) = T(s) = W_m(s) = \frac{y_m}{r}(s) .$$

With the above control law, the closed-loop complementary sensitivity is given by

$$T = \frac{c_0 k_p Z_p \Lambda^2}{\Lambda[(\Lambda - \theta_1{}^{\mathrm{T}}\alpha) R_p - k_p Z_p (\theta_2{}^{\mathrm{T}}\alpha + \theta_3 \Lambda)]} = k_m \frac{Z_m}{R_m} . \quad (5)$$

By choosing

$$c_0 = \frac{k_m}{k_p} , \quad (6)$$

(5) can be written as the Bézout identity

$$\theta_1{}^{\mathrm{T}}\alpha R_p + k_p Z_p (\theta_2{}^{\mathrm{T}}\alpha + \theta_3 \Lambda) = \Lambda R_p - Z_p \Lambda_0 R_m$$

which again can be expressed as

$$S\bar{\theta}_c = p \quad (7)$$

where $\bar{\theta}_c = [\theta_1{}^{\mathrm{T}}, \theta_2{}^{\mathrm{T}}, \theta_3]^{\mathrm{T}}$ and S is a $(2n_p - 1) \times (2n_p - 1)$ Sylvester matrix that depends on the coefficients of the polynomials R_p, $k_p Z_p$ and Λ, and p is a $(2n_p - 1)$ vector with the coefficients of the polynomial $\Lambda R_p - Z_p \Lambda_0 R_m$.

Having learnt the uncertain plant parameters θ of $G_p(s)$ and chosen a reference model $W_m(s)$ and an output filter $1/\Lambda(s)$, the control law parameters θ_c is determined by using the parameter mapping $\theta \to \theta_c$ defined by (6) and (7).

C. Adaptive Law

The indirect MRAC scheme requires the application of a normalized adaptive law, which is necessary for the stability properties of the indirect MRAC scheme, according to Theorem 6.6.2 in [4]. Normalization ensures boundedness of the measured signals used in the adaptive law.

Applicable (normalized) adaptive laws include the gradient method based on either instantaneous or integral cost functions, and the least-squares method [4]. These three methods were implemented and assessed, and for the system at hand all three methods provided reasonable parameter convergence, given that the signals used were carefully prefiltered. The gradient method based on the integral cost function behaves similarly to the least-squares method, but with the added benefit of user selectable convergence rate, and was therefore chosen to be used in the MRAC scheme.

1) Integral Adaptive Law: It is assumed that the measured response z of the system can be described using a vector of model parameters θ appearing affinely with a vector of known signals, φ, called the regressor

$$z = \theta^{\mathrm{T}} \varphi . \quad (8)$$

The objective is to find an estimate of the vector of parameter values, $\hat{\theta}$. By computing the estimated response

$$\hat{z} = \hat{\theta}^{\mathrm{T}} \varphi$$

the estimate error ε can be formed as

$$\varepsilon = \frac{z - \hat{z}}{m^2}$$

where m^2 is a normalization signal (defined below). The estimate of the parameters is obtained by minimizing the cost-function

$$J(\hat{\theta}) = \frac{1}{2} \int_0^t \mathrm{e}^{-\kappa(t-\tau)} \varepsilon^2 m^2 \, \mathrm{d}\tau , \quad (9)$$

where a forgetting factor $\kappa > 0$ is introduced to discount past data in order to achieve exponential convergence. Applying the gradient method, $\dot{\hat{\theta}} = -\Gamma \nabla J(\hat{\theta})$, to find the minimum of (9) results in the recursive expressions

$$\begin{aligned} \dot{\hat{\theta}} &= -\Gamma(R\hat{\theta} + Q) , \ \hat{\theta}(0) = \hat{\theta}_0 \\ \dot{R} &= -\kappa R + \frac{\varphi \varphi^{\mathrm{T}}}{m^2} , \ R(0) = 0 \\ \dot{Q} &= -\kappa Q - \frac{z\varphi}{m^2} , \ Q(0) = 0 \end{aligned}$$

where $\Gamma = \Gamma^{\mathrm{T}} > 0$ is the adaptive gain, and the normalization signal m^2 is constructed as

$$m^2 = 1 + {n_s}^2 \ , \ {n_s}^2 = \alpha_0 \varphi^{\mathrm{T}} \varphi \ , \ \alpha_0 > 0 \ .$$

This method has the properties $\varepsilon, \varepsilon n_s, \hat{\theta}, \dot{\hat{\theta}}, P \in \mathscr{L}_\infty$, $\varepsilon, \varepsilon n_s, \dot{\hat{\theta}} \in \mathscr{L}_2$, and $\lim_{t\to\infty} |\dot{\hat{\theta}}| = 0$. The method has the formal property that if the regressor φ is persistently exciting (PE), and $n_s, \varphi \in \mathscr{L}_\infty$, then $\hat{\theta}$ will converge exponentially to θ, and for $\Gamma = \gamma I$, the convergence rate can be made arbitrarily large by increasing the value of γ.

A piecewise continuous signal vector $\varphi : \mathbb{R}^+ \to \mathbb{R}^n$ is said to be PE in $\mathbb{R}^n$ with a level of excitation $\alpha_0 > 0$ if there exist constants $\alpha_1, T_0 > 0$ such that

$$\alpha_1 I \geq \frac{1}{T_0} \int_t^{t+T_0} \varphi \varphi^{\mathrm{T}} \, \mathrm{d}\tau \geq \alpha_0 I, \ \forall t \geq 0 \ .$$

For linear single-input-single-output systems, such as the one at hand, a PE regressor vector is obtained if the input signal u_p is sufficiently rich. In brief, an input signal is sufficiently rich if it contains more frequency components than half the number of unknown parameters [4].

Lastly, to avoid pure numerical differentiation when estimating parameters of an linear differential equation of degree n, the output z and regressor vector φ should be filtered [4], [13] by a filter with relative degree $n_f^\star \geq n$.

IV. Design Choices

A. Control Law

Assuming good knowledge of the plant model $G_p(s)$, there are two main design choices with regards to the control law, which is the choice of the reference model $W_m(s)$ and the output filter $1/\Lambda(s)$. The main limiting factor in determining these filters, is the uncertainty of the plant model, which for the system at hand is due to non-modeled high-frequency dynamics. The control law from Section III-B can also be expressed in terms of the feed-forward filter

$$C(s) = \frac{c_0 \Lambda(s)}{\Lambda(s) - {\theta_1}^{\mathrm{T}} \alpha(s)}$$

and feedback filter

$$F(s) = -\frac{{\theta_2}^{\mathrm{T}} \alpha(s) + \theta_3 \Lambda(s)}{c_0 \Lambda(s)} \ ,$$

i.e., the control law can be written as

$$u_p = C(s)(r - F(s) y_p) \ .$$

The complementary sensitivity function for a set of nominal plant parameter estimates can then be found as

$$T(s) = \frac{C(s) G_p(s)}{1 + C(s) F(s) G_p(s)} .$$

Since $T(s) = W_m(s)$, the stability criterion

$$\| F(s) W_m(s) \delta_m(s) \|_\infty < 1 \qquad (10)$$

can be used to choose $W_m(s)$ and $1/\Lambda(s)$ to obtain robustness against uncertain dynamics.

For simplicity, the reference model $W_m(s)$ was chosen to be a seventh-order Butterworth filter with cut-off frequency ω_m, i.e., $q_m = 0$ and $p_m = 7$, and since the plant model $G_p(s)$ does not have any zeros, the polynomial $\Lambda(s)$ should be of degree $n_p - 1 = 6$, and the zeros of $\Lambda(s)$ was chosen to have a Butterworth pattern with radius ω_l.

TABLE II

Control law parameter tuning.

ω_c	$2\pi \cdot 1100$	rad/s
ω_m	$2\pi \cdot 900$	rad/s
ω_l	$2\pi \cdot 900$	rad/s

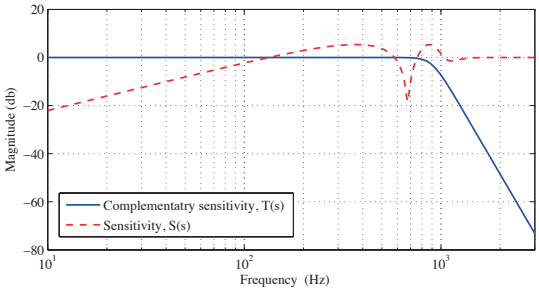

Fig. 7. Nominal response of the complementary sensitivity function and the sensitivity function.

The plant model includes the reconstruction and anti-aliasing filters, $W_r(s)$ and $W_a(s)$, both having the user-programmable cut-off frequency ω_c. As already noted, including these filters as an extra degree of freedom in the tuning of the controller, the filters can be used to improve the nominal tuning of the closed-loop sensitivity and robustness properties, and to attenuate quantization and sensor noise, given that ω_c is below the Nyquist frequency.

The nominal tuning of the control law depends on the choice of ω_m, ω_l, and ω_c. As the plant is open-loop stable, and since it is augmented with an integral state, the performance in terms of the sensitivity function

$$S(s) = \frac{1}{1 + C(s) F(s) G_p(s)}$$

of the nominal closed-loop system is improved by choosing a bandwidth as high as possible for the reference model $W_m(s)$ and the output filter $1/\Lambda(s)$, i.e., choosing ω_m and ω_l as high as possible. The choice of ω_c is not as straight forward, as there can be found an optimal value which minimizes $\|S(s)\|_\infty$. By a course grid search over ω_m, ω_l, and ω_c, evaluating (10) when using the nominal parameters for the two payload configurations from Tab. I, an approximate optimal value for ω_c, and the approximate highest bandwidth for $W_m(s)$ and $1/\Lambda(s)$ without violating (10) was determined, and the result is shown in Tab. II. The nominal frequency responses of the complementary sensitivity function $T(s)$ and the sensitivity function $S(s)$ using the parameters in case 1) in Tab. I are shown i Fig. 7. As can be seen, the expected bandwidth is approximately 90 Hz.

B. Adaptive Law

For the adaptive law, values for the forgetting factor κ, the normalization constant α_0, and the gains Γ, must be selected. Also, the adaptive law will theoretically provide convergence

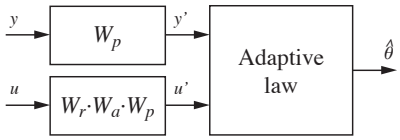

Fig. 8. Signal filtering configuration for the adaptive law.

to the correct parameter values when using a sufficiently rich input signal (which results in a PE regressor vector) [4], [14]. For the system at hand, none of the three methods provided reasonable parameter convergence without careful pre-filtering of the signals used. Thus, a pre-filter $W_p(s)$ must also be selected.

The main limitation for the selection of κ, α_0, and Γ is the numerical stability of the adaptive law. If either κ or Γ are too large, or if α_0 is too small, depending on the selected numerical integration scheme and step size, the adaptive law can become unstable. As long as the adaptive law remains stable, the choice of κ, α_0, and Γ will not influence the mean values of the stationary response for the estimated parameter values. The mean values will mostly depend on the pre-filter $W_p(s)$. However, the choice of κ, α_0, and Γ determines the rate of adaptation and amount of averaging, and thus how much fluctuation there will be in the estimates due to noise and other disturbances.

The choice of the pre-filter is done considering the concepts of dominantly rich signals and experiment design, as they provide guidance on how to choose input signals that should provide better parameter estimates under non-ideal conditions.

The deterministic concept of dominantly rich signals [4] provides conditions on the choice of an input signal in the presence of non-modeled dynamics and bounded disturbances, in order to obtain small biases in the parameter estimates. Summarily, the input signal should be chosen to excite the dominant dynamics of the system to a level that dominates the disturbances, and have a spectral content that avoids excitation of umodeled dynamics.

Somewhat similarly, the stochastic concept of experiment design [15], [16], provides methods to construct input signals of finite power that will maximize conditions on the Fisher information matrix, which should then provide parameter estimates with minimal variance when using measurements corrupted by colored noise. The Fisher information matrix in the frequency domain involves the parameter sensitivity functions for the plant model. A finite energy signal will then typically be optimal for some condition on the information matrix if the spectral content is concentrated in frequency domains where the parameter sensitivity functions of a model have peaks. An optimal input signal in this sense should also improve the convergence rate of the parameter estimates [17].

As designing an optimal input signal is usually not feasible for arbitrary tracking control tasks, a practically feasible solution is to find a pre-filter which emphasizes certain frequency domains in the signals used in the parameter identification scheme [6], [14], [18]. In addition to provide more optimal signals with regards to the information matrix, the pre-filter is also beneficial since it can attenuate disturbances and non-modeled effects; thus a more dominantly rich signal.

A heuristic approach is chosen in order to select a reasonable pre-filter $W_p(s)$. As prior knowledge of approximate parameter values is available from frequency response data, a nominal model reference controller (MRC) is found. Data collected from the plant while running in closed-loop using the MRC then provide a reasonable approximation to the expected input signal and noise correlation when using the MRAC. Using these data off-line, different filter choices are tested, according to the following considerations.

As was demonstrated in [18], the parameter sensitivities of a mass-spring-damper system suggest an emphasis on a frequency domain around the expected dominant resonant frequency of the system; a bandpass filter. As the scheme requires differentiation of the measured deflection, the bandpass filter must have a relative degree equal to the highest order of differentiation needed, so that the filters will be proper. To provide some low-pass filtering, the relative degree should be higher. Choosing only a bandpass filter $W_1(s)$ with a narrow passband around expected resonant frequency results in poor low-frequency gain estimation for this system, i.e., the ratio b_0/a_0 is too low. Adding another bandpass filter in parallel, with a narrow passband around the fundamental frequency of the reference signal and a selectable gain $k_2 W_2(s)$, increases the parameter identification accuracy. The gain k_2 can not be too large, as it will impact the accuracy of parameters depending on the natural frequency and damping coefficient, a_1 and a_0. The filter that is used is thus

$$W_p(s) = W_1(s) + k_2 W_2(s)\,, \tag{11}$$

where the cut-off frequencies for $W_1(s)$ is $[f_1^l, f_1^h] = [475, 900]$ and for $W_2(s)$ is $[f_2^l, f_2^h] = [f_r - 10, f_r + 10]$, f_r being the fundamental frequency of the reference signal. The filter gain was chosen to be $k_2 = 0.01$. The chosen pre-filter is shown in Fig. 9.

For the model (1), assuming a displacement measurement y_d, the parameter vector in the parametric model (8) is

$$\theta_p = [b_0, a_1, a_0]^{\mathrm{T}},$$

and the regressor vector is

$$\varphi = [u_a, -\dot{y}_d, -y_d]^{\mathrm{T}},$$

and the output of the model is $z = \ddot{y}_d$. To account for the known dynamics in the reconstruction and anti-aliasing filters, determined by the cut-off frequency ω_c, and incorporating the pre-filter, the output z and regressor φ is constructed as

$$z(s) = s^2 W_p(s) y_p$$

and

$$\varphi(s) = [W_r(s) W_a(s) W_p(s) u_p, -s W_p(s) y_p, -W_p(s) y_p]^{\mathrm{T}},$$

as illustrated in Fig. 8.

Reasonable values for κ, α_0, and Γ, trading-off convergence rate and forgetting rate (averaging), were found as $\kappa = 2$, $\alpha_0 = 0.001$, and

$$\Gamma = \mathrm{diag}([5 \cdot 10^6, 5 \cdot 10^1, 5 \cdot 10^7])\,.$$

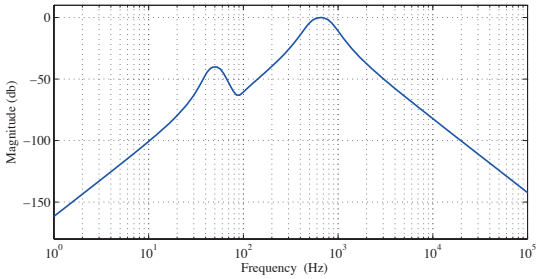

Fig. 9. Pre-filter $W_p(S)$.

The parameter vector θ, is determined by the convolution of the polynomials in the numerator and denominator of $W_r(s)$, $W_a(s)$, and $G_p(s)$, and the parameter mapping from the adaptive law to the control parameters is $\theta_p \rightarrow \theta \rightarrow \theta_c$.

V. EXPERIMENTAL RESULTS

A. Description of the Experimental System

The experimental set-up consisted of a Dell Optiplex 760 computer equipped with a PCI-6221 data acquisition board from National Instruments, running the xPC Target real-time operating system for hardware-in-the-loop simulations, a ADE 6810 capacitive gauge and ADE 6501 capacitive probe from ADE Technologies, a Piezodrive PDL200 voltage amplifier, the custom-made long-range serial-kinematic nanopositioner (see Fig. 2), two SIM 965 programmable filters, and a SIM983 scaling amplifier from Stanford Research Systems. With the xPC Target, a maximum sampling frequency of $f_s = 40$ kHz was achieved for the complete MRAC scheme, and used for all the experiments. For numerical integration, a third-order Runge-Kutta scheme (Bogacki-Shampine) was used. In order to achieve a higher sampling frequency, the adaptive law and parameter mapping was implemented using the C programming language.

B. Experiments

Four experiments were performed to assess the tracking and parameter estimation performance. A triangular reference signal with a fundamental frequency $f_r = 50$ Hz was used, which is quite common for SPM applications, and it is sufficiently rich for parameter estimation for this system. The control bandwidth is approximately 90 Hz, thus using a relatively high fundamental frequency should help elucidate model discrepancies and disturbances in the system response. First, the ability to track parameter changes is evaluated by adding a payload of 15.7 g while the system is running. Next, three experiments were done to find the asymptotic parameter estimates for various configurations, as well as the stationary tracking error.

C. Results and Discussion

The experimental results are presented in Figs. 10 and 11, and Tab. III.

From Fig. 10 it is evident that reasonable parameter convergence is achieved, and the adaptive law is able to track parameter changes when the payload is added after approximately 5 seconds. There are discrepancies in the estimates compared to the values in Tab. I, especially for the b_0 and a_1 parameters. The discrepancy for b_0 is mainly due to the larger driving voltage amplitude used in the experiment, compared to the amplitude used to find the frequency response. The discrepancy for a_1 is likely due to the presence of colored noise due to feedback and the hysteresis disturbance, since the parameter sensitivity for the model (1) with respect to a_1 is very small, as was pointed out in [18]. The small fluctuations in the a_1 estimate is due to noise, and can be reduced by decreasing e.g. the corresponding gain in Γ, at the expense of slower convergence.

TABLE III

ASYMPTOTIC VALUES FOR THE ESTIMATES FOR THE PARAMETERS IN THE MODEL (1) AND STATIONARY TRACKING ERRORS FOR THE MRAC SCHEME FOR VARIOUS CONFIGURATIONS.

1) No payload; 50 Hz, 3 μm amp. triangle wave ref.					
b_0	$2.79{\cdot}10^6$	μm/s^{2}V	b_0/a_0	0.130	μm/V
a_0	$21.4{\cdot}10^6$	1/s^2	f_0	737	Hz
a_1	297	1/s	ζ	0.0321	-
RMSE:		0.113 μm	RMSE relative:		6.52 %
Max. error:		0.213 μm	Max. relative error:		7.31 %
2) Payload; 50 Hz, 3 μm amp. triangle wave ref.					
b_0	$2.33{\cdot}10^6$	μm/s^{2}V	b_0/a_0	0.131	μm/V
a_0	$17.8{\cdot}10^6$	1/s^2	f_0	672	Hz
a_1	32.9	1/s	ζ	0.00390	-
RMSE:		0.101 μm	RMSE relative:		5.82 %
Max. error:		0.186 μm	Max. relative error:		6.40 %
3) Payload; 50 Hz, 6 μm amp. triangle wave ref.					
b_0	$2.46{\cdot}10^6$	μm/s^{2}V	b_0/a_0	0.144	μm/V
a_0	$17.1{\cdot}10^6$	1/s^2	f_0	657	Hz
a_1	-95.0	1/s	ζ	-0.0115	-
RMSE:		0.282 μm	RMSE relative:		8.15 %
Max. error:		0.520 μm	Max. relative error:		8.94 %

By inspection of case 1) and 2) in Tab. III, it can seen that the estimates for the natural frequency and the damping ratio is underestimated in case 1), and overestimated in case 2). This is likely due to the tuning of the pre-filter, as the bias change, and the accuracy improves, by fine tuning of the pre-filter to the specific configuration. Case 2) and 3) demonstrate the ability to track the change in low-frequency gain b_0/a_0 due to change in displacement range, as should be expected by the results in Fig. 4, but there is also a noticeable change in the estimated natural frequency and damping ratio, which also depend on the pre-filter tuning.

As already noted in Section IV-B, the low-frequency gain is always underestimated. This can be seen by looking at Fig. 11, where it is apparent that the system response overshoots the reference. This can be confirmed by fixing the parameter estimates and manually increasing the b_0 estimate, in which case the error can be reduced.

VI. CONCLUSIONS AND FUTURE WORKS

A. Conclusions

A working implementation of a MRAC scheme has been demonstrated, and the experimental results obtained provide an indication of the achievable performance that can be expected when applied to a flexible smart structure. The main challenge was to achieve reasonable convergence for the parameter estimation scheme, and this was demonstrated

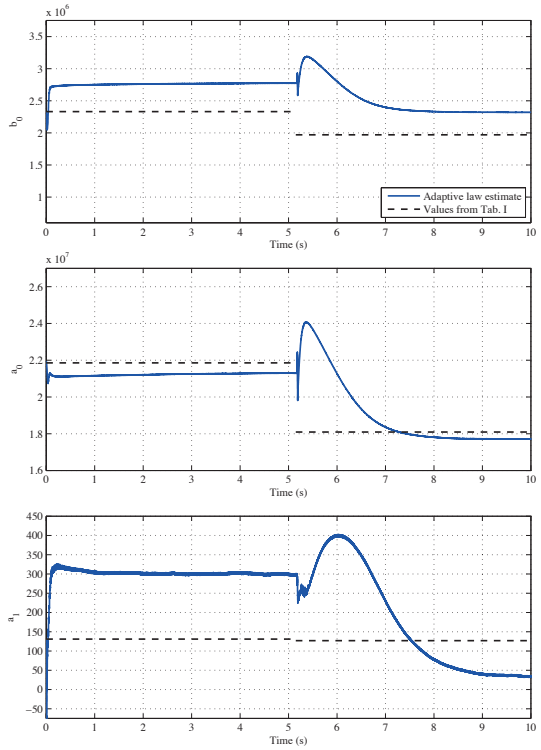

Fig. 10. Estimated parameters when adding a payload to the sample platform, using a 50 Hz triangle wave reference signal with 3 μm amplitude.

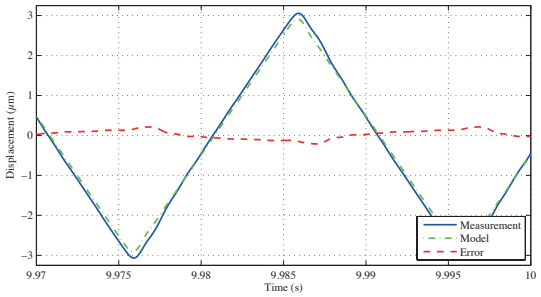

Fig. 11. Stationary response, with payload on the sample platform, using a 50 Hz triangle wave reference signal with 3 μm amplitude.

to be possible by the use of a special pre-filter. One major limitation with regards to performance is the difficulty in having simultaneous accurate estimation of the parameters determining the low-frequency gain and the parameters dependent on the damping ratio and natural frequency of the system. This is most likely due to the presence colored noise due to feedback and the disturbance introduced due to hysteresis. The disturbance due hysteresis and creep also necessitates integral action in the controller. The suppression of these disturbances are dependent on the achievable controller bandwidth, which main limiting factor is the presence of non-modeled and practically uncontrollable higher-order vibration modes.

B. Future Works

The parameter estimation is very sensitive to the choice of pre-filter $W_p(s)$, the actual plant parameters, the chosen control law parameters, and reference signal. To improve on the parameter estimation performance, it might be possible to find better choices for $W_p(s)$, and the application of more elaborate identification schemes, specifically tailored for closed-loop identification such as the recursive instrumental variable method [13], should be investigated.

In order to make the control scheme more robust in general, well known techniques such as parameter projection and adaptation dead-zones should be used to avoid large parameter drift. Since integral action is added to the control law, a suitable anti-windup scheme should also be added.

VII. ACKNOWLEDGMENTS

The authors would like to thank Brian J. Kenton and Dr. Kam K. Leang for providing the positioning stage, and Dr. Andrew J. Fleming for providing the voltage amplifier.

REFERENCES

[1] S. M. Salapaka and M. V. Salapaka, "Scanning Probe Microscopy," *Control Systems, IEEE*, vol. 28, no. 2, pp. 65–83, Apr. 2008.

[2] G. M. Clayton, S. Tien, K. K. Leang, Q. Zou, and S. Devasia, "A Review of Feedforward Control Approaches in Nanopositioning for High-Speed SPM," *Journal of Dynamic Systems Measurement and Control, Transactions of the ASME*, vol. 131, no. 6, p. 061101, 2009.

[3] S. Devasia, E. Eleftheriou, and S. O. R. Moheimani, "A Survey of Control Issues in Nanopositioning," *Control Systems Technology, IEEE Transactions on*, vol. 15, no. 5, pp. 802–823, 2007.

[4] P. A. Ioannou and J. Sun, *Robust Adaptive Control*. Prentice Hall, Inc., 1995.

[5] Y. Stepanenko and C.-Y. Su, "Intelligent Control of Piezoelectric Actuators," in *37th Conference on Decision and Control, Proceedings of the*, Tampa, FL, Dec. 1998, pp. 4234–4239.

[6] R. Middleton, G. C. Goodwin, D. Hill, and D. Q. Mayne, "Design issues in adaptive control," *Automatic Control, IEEE Transactions on*, vol. 33, no. 1, pp. 50–58, 1988.

[7] Y. Li and J. Bechhoefer, "Feedforward control of a closed-loop piezoelectric translation stage for atomic force microscope," *Review of Scientific Instruments*, Jan. 2007.

[8] D. Berlincourt, B. Jaffe, H. Jaffe, and H. Krueger, "Transducer Properties of Lead Titanate Zirconate Ceramics," *Ultrasonic Engineering, IRE Transactions on*, vol. 7, no. 1, pp. 1–6, Jan. 1960.

[9] S. Hudlet, M. Saint Jean, D. Royer, J. Berger, and C. Guthmann, "In situ measurement of large piezoelectric displacements in resonant atomic force microscopy," *Review of Scientific Instruments*, vol. 66, no. 4, p. 2848, 1995.

[10] A. Pramanick, D. Damjanovic, J. C. Nino, and J. L. Jones, "Subcoercive Cyclic Electrical Loading of Lead Zirconate Titanate Ceramics I: Nonlinearities and Losses in the Converse Piezoelectric Effect," *Journal of the American Ceramic Society*, vol. 92, no. 10, pp. 2291–2299, Oct. 2009.

[11] N. Hovakimyan and C. Cao, $\mathcal{L}_1$ *Adaptive Control Theory: Guaranteed Robustness with Fast Adaptation*. Society for Industrial and Applied Mathematics, 2010.

[12] M. Krstic, I. Kanellakopoulos, and P. V. Kokotovic, *Nonlinear and Adaptive Control Design*. Wiley-Interscience, 1995.

[13] H. Garnier and L. Wang, Eds., *Identification of Continuous-time Models from Sampled Data*. Springer, 2008.

[14] L. Ljung, *System Identification: Theory for the User*, 2nd ed. Prentice Hall, Inc., 1999.

[15] G. C. Goodwin and R. L. Payne, *Dynamic System Identification: Experiment Design and Data Analysis*. Academic Press, 1977.

[16] C. R. Rojas, J. S. Welsh, G. C. Goodwin, and A. Feuer, "Robust optimal experiment design for system identification," *Automatica*, vol. 43, no. 6, pp. 993–1008, June 2007.

[17] I. M. Y. Mareels, M. Gevers, R. R. Bitmead, C. R. Johnson, R. L. Kosut, and M. A. Poubelle, "How exciting can a signal really be?" *Systems & Control Letters*, vol. 8, no. 3, pp. 197–204, 1987.

[18] A. A. Eielsen, T. Polóni, T. Johansen, and J. T. Gravdahl, "Experimental Comparison of Online Parameter Identification Schemes for a Nanopositioning Stage with Variable Mass," in *Advanced Intelligent Mechatronics, IEEE/ASME International Conference on*, Budapest, July 2011, pp. 510–517.